Egypt. J. Chem. **Vol. 68,** SI: Z. M. Nofal, pp. 911 - 921 (2025)

Egyptian Journal of Chemistry

http://ejchem.journals.ekb.eg/

Antibacterial Potential of Ag–Au Alloy Nanoparticles Combined with Femtosecond Laser Light against Drug-Resistant Eye Pathogens

Ahmed O. El-Gendy [1,2], Talal Hussein [1,3], Esraa Ahmed [1], Ola Dabbous [4], Tarek Mohamed [1,5,*]

[1]*Laser Institute for Research and Applications LIRA, Beni-Suef University, Beni-Suef 62511, Egypt*
[2]*Faculty of Pharmacy, Department of Microbiology and Immunology, Beni-Suef University, Beni-Suef 62514, Egypt*
[3]*Anbar Health Department, Anbar province, Ministry of Health, Iraq*
[4]*Department of Medical Applications of Laser, National Institute of Laser Enhanced Sciences (NILES), Cairo University, Giza, Egypt*
[5]*Department of Engineering, Faculty of Advanced Technology and Multidiscipline, Universitas Airlangga, Indonesia*

Abstract

The synthesis of bimetallic nanoparticles (BNPs) has garnered significant interest due to their superior physicochemical and biological properties compared to monometallic nanoparticles (MNPs). In this study, Ag/Au alloy nanoparticles were synthesized via pulsed laser ablation in liquid (PLAL) and characterized for their optical, morphological, and antibacterial properties. The formation of Ag/Au alloy nanoparticles was characterized through UV-Vis spectroscopy, transmission electron microscopy (TEM), and inductively coupled plasma (ICP) analysis. The antibacterial efficacy of the synthesized nanoparticles was evaluated against Methicillin-Resistant Staphylococcus aureus (MRSA) in vitro. Additionally, a femtosecond laser at 400 nm wavelength was employed to assess the synergistic effects of laser irradiation and Ag/Au alloy nanoparticles on bacterial viability. Growth kinetics analysis revealed that femtosecond laser treatment alone significantly reduced bacterial proliferation ($P < 0.0001$), whereas Ag/Au alloy nanoparticles required higher concentrations to exhibit noticeable antibacterial effects. The combination of both approaches resulted in the most pronounced bacterial growth inhibition. This study unlocked a new perception of synthesizing Ag/Au alloy nanoparticles via the laser ablation technique and their potential application in treating various ocular infections particularly when used in conjunction with femtosecond laser-based antimicrobial photodynamic therapy. To our knowledge, this is the first study to report the combined use of femtosecond laser irradiation and PLAL-synthesized Ag/Au alloy NPs for antimicrobial photodynamic therapy, offering a novel approach to combating drug-resistant eye pathogens. Further studies are needed to optimize the synthesis parameters and evaluate the biocompatibility of these nanoparticles for future clinical applications.

Keywords: Eye infection; Laser ablation, antibacterial, Ag/Au alloy nanoparticles, Biocompatibility, photodynamic therapy, Gram-positive bacteria, Femtosecond laser, Quantum dots, MRSA.

1. Introduction

Monometallic nanoparticles (MNPs) have attracted considerable interest from researchers due to their exceptional optical, biological, electrical, and chemical properties [1-3]. In contrast, bimetallic nanoparticles (BNPs) have opened new avenues by offering superior features compared to MNPs, thanks to their synergistic effects [4]. The shape, size, and composition of BNPs significantly influence their electrical, biological, optical, and catalytic properties, providing enhanced stability and diffusion by fine-tuning the plasmonic band with an added degree of flexibility [4,5]. Notably, BNPs generally demonstrate greater catalytic efficiency and selectivity than MNPs, especially in catalytic reaction processes [5]. Compared to MNPs, BNPs have garnered greater interest due to the dual functionalities offered by each metallic component, along with enhanced or newly discovered properties that hold significant application potential [5]. Ag/Au bimetallic nanoparticles have garnered considerable interest owing to their exceptional and unique properties [4-6]. Ag/Au alloy NPs have been utilized in many areas, such as antibacterial [7], drug delivery, cancer therapy [8], and nanoscale optical biosensors [9]. Currently, there are various methods of synthesizing NPs, the most employed among them being chemical techniques [10,11]. However, these techniques have their drawbacks, one of which is their toxicity. The most efficient approach is to use lasers, which are more effective due to their ability to precisely control the laser radiation parameters, which helps to produce NPs with the proper composition and morphology. The most widely used are laser ablation methods in liquid, vacuum, or gas [12-17]. Laser ablation is a physical method for nanoparticle synthesis that operates predominantly through a top-down approach, where nanoscale clusters are formed by removing small particles, such as atoms or ions, from a bulk material. In laser-based procedures, the bulk material is heated to a high temperature using a laser, and then the vapors condense to produce nanoparticles [18]. Severe ocular infections caused by bacteria, viruses, fungi, or parasites can lead to visual impairments or

*Corresponding author e-mail: tarek_mohamed1969@lira.bsu.edu.eg; (Tarek Mohamed).
Received date 10 April 2025; Revised date 24 May 2025; Accepted date 05 July 2025
DOI: 10.21608/ejchem.2025.374399.11575

blindness if not properly treated [1,2]. Gram-positive and Gram-negative bacterial pathogens collectively account for approximately 32% to 74% of eye infections globally [3,4]. The risk of developing an eye infection depends on the specific type of bacterial pathogen involved [5]. *Staphylococcus aureus* is recognized worldwide as one of the most prevalent Gram-positive bacteria linked to ocular infections [6,7]. Due to the continual overuse and misuse of antibacterial medications, bacterial pathogens are developing antibiotic resistance at a rapid rate [8], which explains the continuous need for cutting-edge alternative antibacterial therapies [9]. Nanomaterial-based therapeutic strategies have recently emerged as a highly promising alternative for antimicrobial applications, attracting considerable attention due to their beneficial biological attributes, including superior biocompatibility, remarkable adsorption capabilities, and the potential for easy surface modification [10]. The antimicrobial activities of diverse metal and metal oxide nanoparticles, including silver, zinc oxide, titanium oxide, and gold, have been the focus of extensive research [11,12]. Seeking a synergistic effect enhances the antibacterial properties while maintaining biocompatibility.

Laser-based antimicrobial photodynamic therapy (lb-aPDT) is another promising treatment strategy, offering a non-invasive approach for effectively eradicating various infections [13]. Building on our earlier research on the bactericidal value of femtosecond laser-based treatment [14,15], as well as the combination therapeutic antibacterial strategy utilizing various NPs generated with PLAL [15-17]. Nanomaterial-based therapeutic strategies have recently emerged as a highly promising alternative for antimicrobial applications, attracting considerable attention due to their biological attributes, including superior biocompatibility, remarkable adsorption capabilities, and easy surface modification [18]. The antimicrobial actions of metal-based nanoparticles such as silver, zinc oxide, and titanium oxide have been investigated against a wide range of pathogens, including fungal species. Notably, silver nanoparticles have also demonstrated antifungal properties, as shown in their activity against *Aspergillus niger*, expanding their antimicrobial spectrum beyond bacteria [18].

In this research, Ag/Au alloy NPs were generated using PLAL, and the effect of irradiating a mixture of the prepared nanoparticles with a pulsed laser at different average powers (500-900) mW and different exposure times (5 - 30 min) was studied as well as some measurements such as optical transmission and absorption, average size, and concentration of Ag/Au alloy NPs were performed. Additionally, the antibacterial efficacy of the synthesized nanoparticles was evaluated in vitro, both independently and in conjunction with femtosecond laser irradiation at a 400 nm wavelength, which lies in the visible spectrum and has shown promising safety and efficacy in previous antimicrobial studies, with an average power of 50 mW and an energy density of 159 J/cm². For the photoactivation experiment, a wavelength of 370 nm was also employed due to its overlap with the absorption peak of Ag/Au alloy NPs, ensuring optimal excitation and potential enhancement of antibacterial effects.

The main objective of this study is to investigate the synergistic antibacterial effects of femtosecond laser irradiation combined with Ag/Au alloy nanoparticles synthesized by PLAL, and to evaluate their potential as a novel therapeutic approach against drug-resistant ocular pathogens

2. Materials and Methods

2.1. Laser ablation and production of TiO2-NPs

As illustrated in Fig. 1, nanoparticles (NPs) were synthesized using standard pulsed laser ablation in water, employing an Nd: YAG laser (Quanta-Ray Pro-350) with a 532 nm wavelength, a 10 ns pulse duration, and a 10 Hz repetition rate. The synthesis of gold/silver alloy nanoparticles was carried out in two stages: first, separate ablation of high-purity (99.99%) square bulk samples of silver and gold, each measuring 20×20×2 mm, was performed using pulsed laser irradiation.

The primary phase focused on the synthesis of Au and Ag nanoparticles, adhering to specific preparatory procedures. This included polishing the bulk Au and Ag samples to detach any oxide layers, ensuring their surfaces were smooth and free of burrs. The polished samples were then subjected to ultrasonic cleaning for 30 minutes using deionized water and ethanol to eliminate any organic residues. Following this, each sample was positioned at the bottommost of a beaker containing 10 ml of purified water, with the beaker securely attached to a monitoring speed device for precise control throughout the process. This device rotates the beaker with the sample together at the same time to avoid engraving the sample or centering the laser beam on the same point during the ablation process. Additionally, the speed had been adjusted to approximately 177 RPM.

A 10.5 cm convex lens was employed in the experimental setup. Additionally, the distance from the sample to the lens at the focus was measured. Furthermore, the diameter of the laser beam at this distance is about 2 mm. At this stage of the experiment, Au and Ag nanoparticles were synthesized by optimizing the exposure time to 30 minutes and the average power to 700 mW. The second step involved the preparation of Au /Ag alloy nanoparticles using the standard setup illustrated in Fig. 1, with the exception that the convex lens was not employed. We added Ag and Au NP solutions at an equal volume ratio of 6 ml to 6 ml (1:1). Next, the combination was re-irradiated by the pulsed laser at various average powers of 500 - 900 mW and various exposure times of 5-30 min. After the preparation of a mixture of Au / Ag alloy NPs, various characteristics were measured, including measuring the optical transmission spectrum by utilizing an ultraviolet-visible spectrophotometer and identifying the structure and average size diffusion of NPs by utilizing the transmission electron microscope. Additionally, the concentration of the colloidal nanoparticles was determined using an inductively coupled plasma (ICP) device.

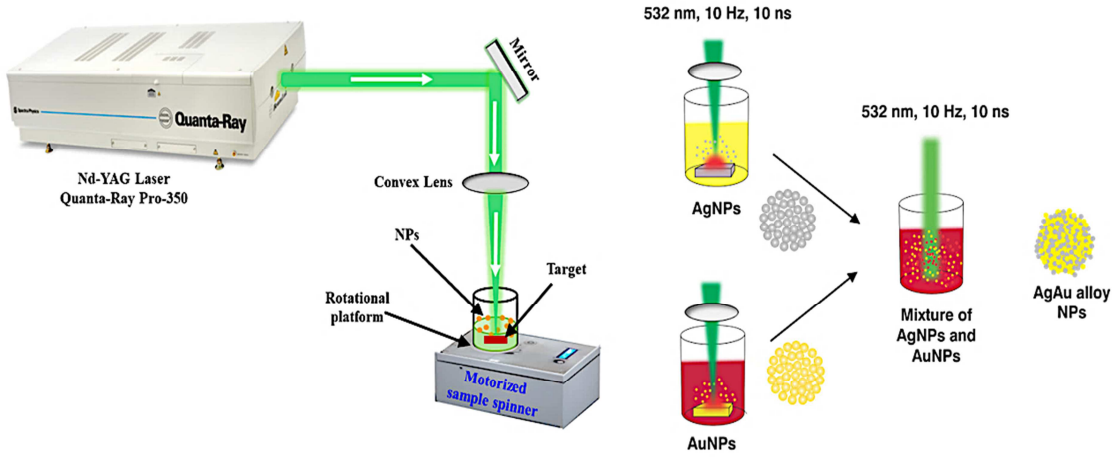

Figure 1: A schematic representation of the setup for the synthesis of monometallic nanoparticles using pulsed laser ablation in liquid

2.2. Microorganism and Cultural Conditions

The Gram-positive bacterial strain investigated in this research is Methicillin Resistant Staphylococcus aureus ATCC 43300 (MRSA), which was cultivated in Brain Heart Infusion (BHI) broth and incubated at 37°C. Before treatment, the microbial suspension's turbidity was adjusted to the 0.5 McFarland standard (approximately 1.5×10^8 CFU/mL). Following this, a 100 µL portion of the prepared suspension was dispensed into a 96-well microplate at specified wells.

2.3. Preparation and Treatment of Bacterial Pathogens Using a Femtosecond Laser System

In this study, a femtosecond mode-locked Ti: sapphire laser (MAI TAI HP, Spectra-Physics) was employed, delivering a typical power of 1.5 – 2.9 W, operating at a repetition rate of 80 MHz, and emitting wavelengths in the 690 – 1040 nm range. This laser served as a pump for the laser system - INSPIRE HF100 (Spectra-Physics), which generated 400 nm femtosecond laser pulses.

As depicted in Fig. 2, a power meter (Newport 843R) was utilized to measure the laser's output power. Positioned 10 cm above overnight-cultured microorganisms in a 96-well microtiter plate, a beam expander with two converging lenses was used to enlarge the laser beam diameter from 2 mm to 10 mm. A laser attenuator (designated A) regulated the power reaching the samples to 50 mW, and an adjustable iris (designated I) controlled the beam diameter. The laser beam was directed toward the samples using mirrors M1 and M2.

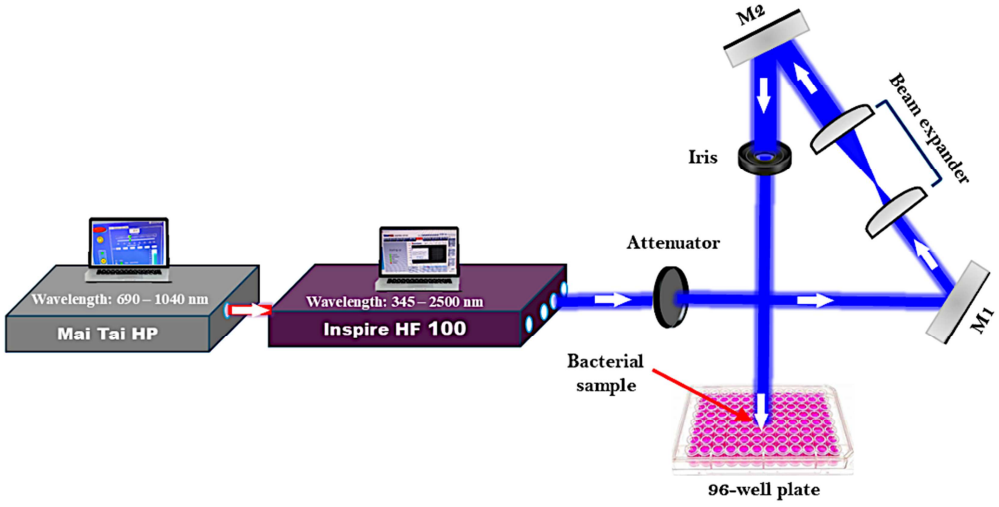

Figure 2: Setup for exposing bacteria to femtosecond laser irradiation. The laser beam was directed toward the samples using mirrors M1 and M2. An attenuator (denoted as A) was used to regulate the laser intensity, adjusting the power to 50 mW directed to the samples. Additionally, to adjust the beam diameter as required for the experiment, an adjustable iris (denoted as I) was used

2.4. Assessment of Growth Kinetics in MRSA Following Femtosecond Laser and/or Au/Ag alloy NPs Treatments

The Au/Ag alloy NPs were mixed at specified concentrations in double-strength BHI broth using a vortex mixer. Following this, 100 µL of the prepared suspension was dispensed into each well of a 96-well microtiter plate. Using a multichannel

pipette, 100 µL aliquots of prepared bacterial cultures, whether laser-treated or untreated (control), were then added to the plate. Each well of the microtiter plate contained bacterial suspensions treated as follows: Laser Treatment, where microorganisms were exposed to femtosecond laser pulses; Au/Ag alloy NPs Treatment, involving the addition of Au/Ag alloy NPs dispersed in BHI broth to bacterial cultures; and Combined Treatment, where bacterial cultures received both laser treatment and Ag/Au alloy NPs simultaneously. Microorganisms without treatment were placed in the positive control wells, while the wells contained only BHI broth represented negative control. After treatment, the plate was incubated for 16 hours at 37°C, during which optical density (OD) readings at a wavelength of 620 nm were taken every 30 minutes using a microplate reader. To evaluate the potential antibacterial capabilities of the Au/Ag alloy NPs, growth curves and the maximum growth rate (µmax) were analyzed. The µmax value was calculated using the following equation: $X_t = X_0 \exp(\mu_{max} . t)$, where X_t represents the absorbance at a specific time point, X_0 is the initial absorbance, and t denotes the time corresponding to $\mu_{max.}$

2.5. Statistical analysis

Data analysis included plotting growth curves to monitor microbial proliferation over time, followed by assessing growth rates and kinetics. Mean values ± standard error was utilized for data representation. Using GraphPad Prism 7 software, one-way ANOVA was performed for statistical comparisons among multiple groups, followed by Tukey's post hoc test. A P-value of less than 0.05 was deemed statistically significant. All experimental procedures were performed in triplicate under sterile conditions.

3. Results and discussion

The transmission spectrum of Au and Ag nanoparticles produced by pulsed laser ablation and examined with a UV-Vis spectrophotometer (Model: C-7200) are shown in Fig. 3. The nanoparticles were exposed for 30 minutes at an average power of 700 mW. Their distinct colloidal coloration indicates variations in composition and microstructure [19]. These nanoparticles exhibit characteristic solution colors, a property arising from free electrons' collective oscillation that is triggered by the incident light's oscillating electromagnetic field, a phenomenon described by Mie theory as surface plasmon resonance (SPR) [20]. As depicted in Fig. 3, the SPR for Au and Ag nanoparticles was apparent at 506 nm and 409 nm, respectively. The nanoparticles' sphere-like morphology is indicated by the appearance of a single SPR peak [21,22].

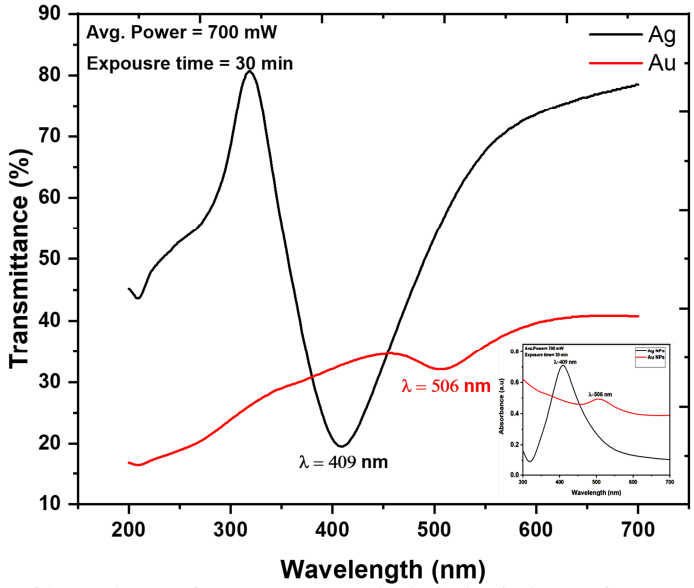

Figure 3: Transmission spectrum of Ag and Au NPs after pulsed laser ablation in liquid with insects of the absorption spectrum

Metal oxide nanoparticles, particularly Ag/Au alloy NPs, have lately garnered interest for their antimicrobial capabilities. Titanium-based nanoparticles also exhibit excellent antibacterial properties and biocompatibility, especially when biosynthesized, making them highly suitable for medical use [23].

Following the completion of the initial step, which involved synthesizing the individual Au and Ag NPs, we moved on to the second step, which involved creating Au/Ag alloy NPs. An equal ratio of 1:1 Au and Ag colloidal NPs was mixed to estimate the interactions between Au and Ag NPs. Additionally, before re-irradiation through a pulsed laser, the transmission spectrum of the combination was measured. Figure 4 illustrates the measured transmission and absorption spectrum of the colloidal Au/Ag alloy NPs combination. As shown, there are two distinct peaks for Au and Ag NPs in the combination. And the bimodal spectrum's peak positions match the Au and Ag NPs' SPR absorption peaks. Due to the various volumes of nanoparticles examined using a spectrophotometer, the absorption spectrum of the Au/Ag nanoparticle colloid mixture was diminished, as shown in Fig. 4. A 2 ml colloidal solution was used to record the transmission spectra of the Au and Ag

nanoparticles. However, for the combined colloid, equal volumes of 1 ml each of the Au and Ag nanoparticle solutions were mixed, ensuring the total volume remained consistent. Reducing the volume of each NP colloidal solution by half resulted in a decline in overall absorption.

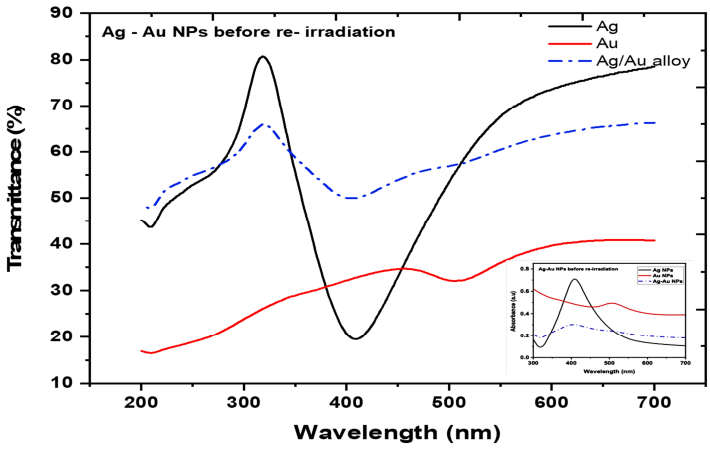

Figure 4: Transmission spectrum of Ag and Au (solid) NPs synthesized by pulsed laser ablation in liquid and the combination of Ag/Au (dished dot) NPs before reirradiation

Experiments were conducted to determine the effects of varying average powers and exposure durations on the formation of Ag/Au alloy NPs following the combination of an equal ratio of Ag to Au NPs. First, at a 15-minute exposure time, the effects of reirradiation of a mixture of Au/Ag NPs with different average powers (500-900 mW) were investigated. Figure 5(a) clarifies the transmission spectrum of Au/Ag alloy NPs at various average powers. At an average power of 500 mW, two clear peaks recognized to Au and Ag NPs, and bandwidth (Δλ) was 178 nm. Additionally, there was a minor blueshift in the SPR for the Au NPs and a redshift in the SPR for the Ag NPs. The change in optical properties of the colloidal solution NPs highlighted the high sensitivity of the UV-Vis absorption spectrums to variations in their morphology and optical properties [24]. At an average power of 700 mW, there was a slight shift in the two absorption peaks of the Au and Ag NPs, and the bandwidth shrank to 135 nm from 500 mW. Furthermore, the bandwidth decreased from 500 to 700 mW to 127 nm upon re-irradiation of the Ag/Au NP mixture at a high average power of 900 mW. A comparatively narrow peak is noticeable at 441 nm. Au/Ag alloy NP production was verified by the gradual alteration of the bimodal peak colloidal to narrow single SPR absorption peak. Numerous studies confirm that a single SPR peak is a reliable indicator of Au/Ag alloy NPs [24-27].
Second, as shown in Fig. 5(b), the effects of various exposure times 5 - 30 min at a constant Avg. power of 700 mW on the re-irradiation of Au/Ag alloy NPs were estimated. At 5 minutes, the absorption peak with a bandwidth (Δλ) of 218 nm significantly broadened, and two separate SPR peaks associated with Ag and Au NPs were visible. When a mixture of Ag and Au NPs was re-irradiated to an exposure time of 15 min, it was found that the bandwidth of the peak dropped to a value of 5 min and accessed 135 nm. Furthermore, there were two peaks attributed to Ag and Au NPs. Additionally, when a mixture was exposed to 30 minutes of radiation, its peak intensity decreased to a level equivalent to that at 15 minutes, and the bandwidth was increased to 129 nm. At 454 nm, a comparatively solitary peak emerged. When the bimodal colloid gradually transformed into a single SPR absorption peak, it was demonstrated that Ag/Au alloys were created.

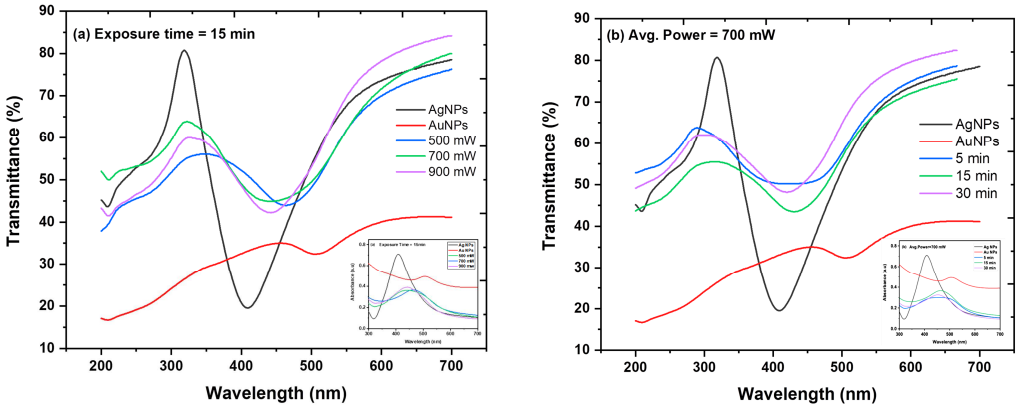

Figure 5: Transmission spectrum of Au/Ag alloy NPs after (a) At fixed exposure time of 15 min and average power ranging from 500 to 900 mW, and (b) At fixed average power of 700 mW and various exposure times from 5 to 30 min.

Using an inductively coupled plasma (ICP) device (Agilent 5100 Synchronous Vertical Dual View (SVDV) ICP-OES, with Agilent Vapour Generation Accessory VGA 77), the concentrations of Au and Ag NPs were determined to be 19.2 and 15 mg/L, respectively. Furthermore, following re-irradiation with the pulsed laser, the concentration of a mixture of Au/Ag colloidal NPs was measured. At 500, 700, and 900 mW various average powers, the mixture's concentrations were 14.8, 17.2, and 15.8 mg/L. At various exposure times 5, 15, and 30 min, the mixture's concentrations were 16.06, 17.2, and 15.34 mg/L. The morphology of the nanoparticles and the average size distribution of Ag and Au NPs have both been examined using the transmission electron microscope (TEM). The spherical shape of the nanoparticles for both Ag and Au samples is depicted in Fig. 6 (a) and (b). The average size of Au NPs is 5.1 nm, while that of Ag NPs is 17.9 nm, according to the size distribution histogram displayed as an inset in each figure. Since Au NPs have distinct physical, chemical, and thermal properties, their average size indicates that we are approaching the quantum dot size, where the material behaves entirely differently.

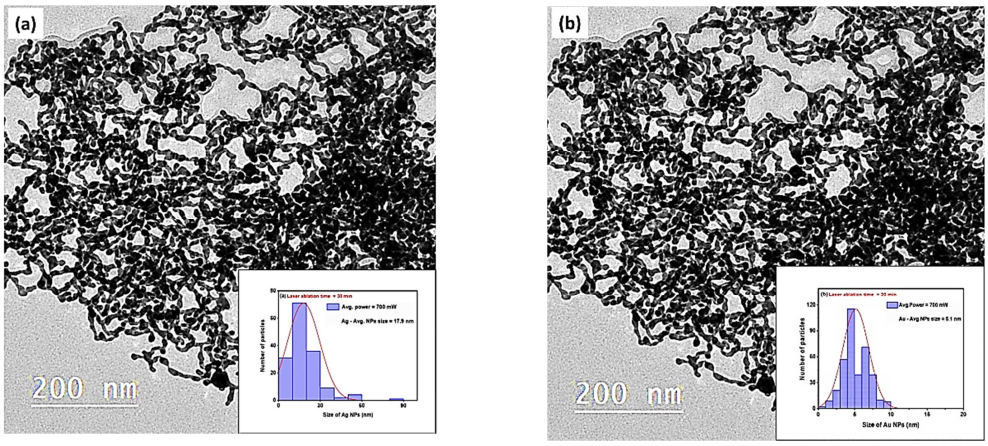

Figure 6: TEM images of the synthesized nanoparticles displayed (a) Ag NPs and (b) Au NPs. The histogram insets in both figures show the size distribution of Ag and Au NPs, respectively

Figures 7 (a), (b), and (c) show both TEM and the average size distribution of the Ag/Au alloy after irradiating the samples to the nanosecond laser at different excitation average power of 500 mW, 700 mW, and 900 mW and at a constant exposure time of 15 min. The results indicate that when the excitation power increases the average size of the NPs decreases from 10.1 nm to 8.5 nm while retaining the spherical shape of the samples.

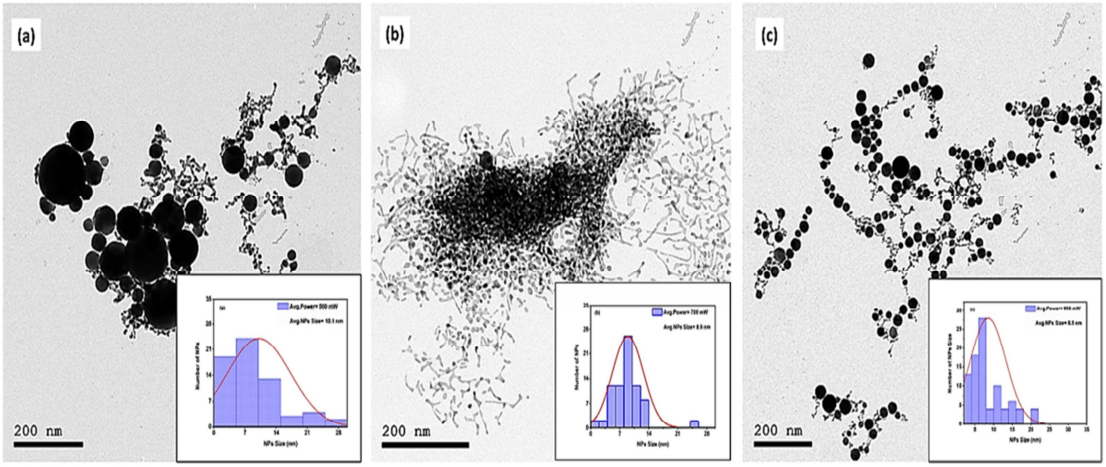

Figure 7: The size distribution histogram for a mixture of Au /Ag NPs at average powers of (a) 500 mW, (b) 700 mW, and (c) 900 mW measured over a 15-minute exposure time. TEM images of the colloidal mixture provide the spherical shape of the Au/Ag NPs alloy

Figure 8 (a, b, and c), shows the effect of the exposure time at a fixed laser excitation power of 700 mW. The finding in Fig. 8 demonstrates that when the exposure time increases from 5 min to 30 min the average size of the nanoparticles decreases gradually from 11.1 nm reaching the quantum dot size of 8 nm at the 30 min exposure time and retaining the spherical shape of the produced nanoparticles.

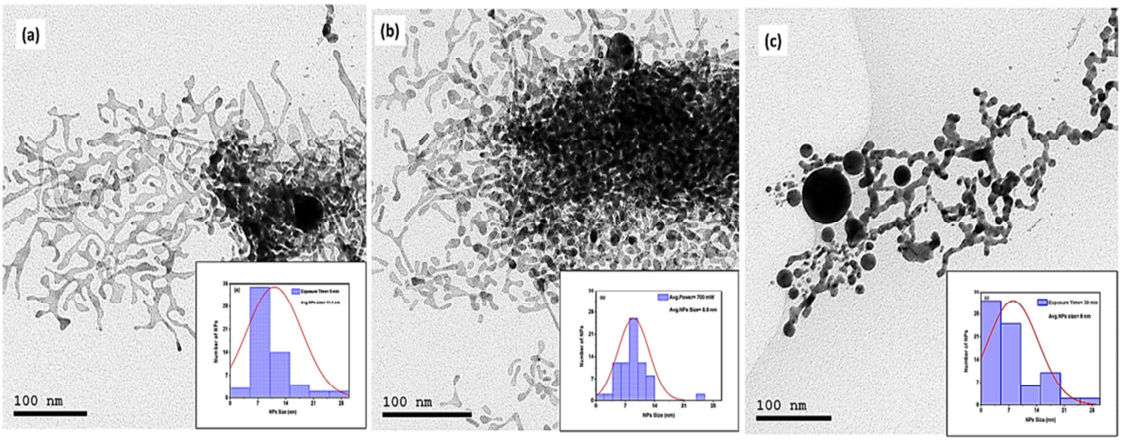

Figure 8: TEM images of the colloidal mixture of an Au/Ag NPs mixture at varying exposure times (a) 5 minutes, (b) 15 minutes, and (c) 30 minutes—under an excitation average power of 700 mW. The corresponding histograms illustrate the size distribution and are presented as insets within the figures

In this study, MRSA samples were subjected to 400 nm femtosecond laser irradiation, which falls within the visible spectrum and is considered comparatively safer for therapeutic use [28,29]. The procedure utilized a final energy density of 159 J/cm², corresponding to an average power of 50 mW and exposure duration of 15 minutes, as illustrated in Fig. 2. It is worth mentioning that energy density, also referred to as fluence (J/cm²), represents the energy applied per unit area [30], and can be calculated as:

$$\text{Energy density} = \frac{\text{Averrage power} \times \text{Exposure duration}}{\text{Spot size } (\pi r^2)}$$

Ag/Au alloy nanoparticles have recently gained attention as a promising alternative in antibacterial therapy due to their enhanced physicochemical properties [31,32]. Several studies have shown that the incorporation of gold into silver nanoparticles can improve their antimicrobial efficacy. Gold contributes to a more controlled and sustained release of Ag^+ ions while simultaneously enhancing the biocompatibility of the resulting nanoparticles [33,34]. As a result, researchers have explored various synthesis strategies to optimize these effects [35].

AuNPs have been widely acknowledged for their applications in biological and medical fields due to their exceptional chemical stability, excellent biocompatibility, minimal acute cytotoxicity, and remarkable catalytic and plasmonic properties [13,36-39]. The antimicrobial properties of nanoparticles are primarily driven by three concurrent mechanisms [40]: (1) disruption of the cell wall and membrane [41], (2) induction of oxidative stress [42], and (3) intracellular component damage [43]. In recent years, bimetallic gold-silver nanoparticles (Au–Ag NPs) have garnered significant attention for their distinctive attributes. Their antibacterial activity, a prominent focus in nanomedicine research, is enhanced by the combination of gold and silver, making them highly effective against bacteria while remaining compatible with human cells [44]. These findings provide valuable insights for tackling drug-resistant bacteria in future studies. Additionally, the incorporation of gold enhances the biocompatibility of these bimetallic nanoparticles. Nonetheless, further investigations are essential to gain a deeper understanding of their mechanisms and to optimize their properties for real-world applications.

The preparation circumstances and laser parameters significantly influence the physicochemical properties of the produced nanoparticles in PLAL. In summary, the present study shows that even though the laser power in PLAL ranged from 500 to 900 mW, with a constant exposure duration of 15 minutes using a 532 nm, 10 Hz nanosecond laser system, the resulting Ag/Au alloy NPs had a consistent particle size within the range of quantum dots (10.1 – 8.5 nm). Yet, the concentration of Ag/Au alloy NPs was highest when the laser power was set at 900 mW.

Our latest study [45] investigated the impact of lb-aPDT on the growth kinetics of S. aureus. We explored how different femtosecond laser parameters might be used to enhance treatment effectiveness and achieve optimal results. In our study, we established that a 15-minute exposure to either a 390 nm or 400 nm femtosecond laser at an average power of 50 mW produced the most pronounced reduction in bacterial viability. Specifically, we treated various microbial cultures with an energy density of 159 J/cm² using a 400 nm femtosecond laser a wavelength within the visible spectrum, regarded as safer for therapeutic applications compared to shorter wavelengths [28,29]. These findings highlight the potential of the safer 400 nm wavelength as a promising option for clinical use. The antimicrobial effects of lasers and other light sources are often attributed to the production of reactive oxygen species (ROS), which play a key role in mediating these effects. ROS are byproducts of cellular oxidative metabolism, and at controlled levels, they exert beneficial effects on cells [11]. However, exposure to external stimuli can cause a significant increase in ROS levels [11]; excessive amount of ROS can have detrimental effects on cell differentiation, signaling, and viability [46].

The impact of a 400 nm femtosecond laser and/or Ag/Au alloy nanoparticles synthesized via laser ablation at varying energy levels on the growth of Methicillin-resistant Staphylococcus aureus (MRSA) was investigated. As illustrated in Fig. 9, the comparative analysis focused on Ag/Au alloy NPs of different average sizes: 10.1 nm (A1), 8.9 nm (A2), 8.5 nm (A3), 11.1

nm (A4), and 8 nm (A5). All samples were maintained at a constant concentration of 13.2 µg/mL, and the growth kinetics of S. aureus was assessed, as shown in Fig. 9. Across all treatment conditions (X-axis), cultures exposed to laser irradiation alone showed significantly reduced bacterial growth rates compared to the untreated control group ($P < 0.0001$, Tukey's test). In contrast, treatment with Ag/Au alloy NPs alone at 13.2 µg/mL did not result in statistically significant differences from the control ($P > 0.05$). These results demonstrate that laser irradiation effectively inhibited the growth kinetics of the tested eye pathogens in vitro, while treatment with NPs alone showed no significant effect, likely due to the relatively low sample concentration of 13.2 µg/mL. The relatively low antibacterial activity observed for Ag/Au alloy NPs alone at a concentration of 13.2 µg/mL may be attributed to several factors. Firstly, the generation of reactive oxygen species (ROS), a critical mediator of nanoparticle-induced bactericidal effects, is often enhanced under photoactivation. Without external irradiation, the intrinsic ROS production by these NPs may be insufficient to induce significant oxidative stress in bacterial cells. Secondly, the interaction kinetics between nanoparticles and bacterial membranes play a key role in antimicrobial efficacy. At sublethal concentrations, nanoparticles may exhibit delayed or limited adhesion and penetration into bacterial cells, reducing their disruptive potential. Furthermore, alloying silver with gold, while beneficial for biocompatibility and NP stability, can modulate the release rate of Ag^+ ions, which are essential for antibacterial action. Gold's inert nature may partially mask the silver surface or alter ion exchange dynamics, thereby attenuating the antimicrobial effect under non-activated conditions [47,48]. Seeking enhancement of the Ag/Au alloy NPs' antibacterial efficacy, we studied the photoactivation of Ag/Au alloy NPs, by exposing them to femtosecond laser before addition to the tested pathogens. The irradiation parameters used for photoactivation were almost the same exposure parameters of the experiment except the wavelength, which was selected to be 370 nm, a wavelength included in the absorption spectrum of the prepared sample, and the growth kinetics of these NPs were compared. This choice was based on the overlap of the 370 nm wavelength with the absorption spectrum of the prepared NPs, allowing for more efficient energy transfer and enhanced interaction with bacterial targets. Again, the effect of Ag/Au alloy NPs was not evident when treated with femtosecond laser compared to sole femtosecond laser treatment.

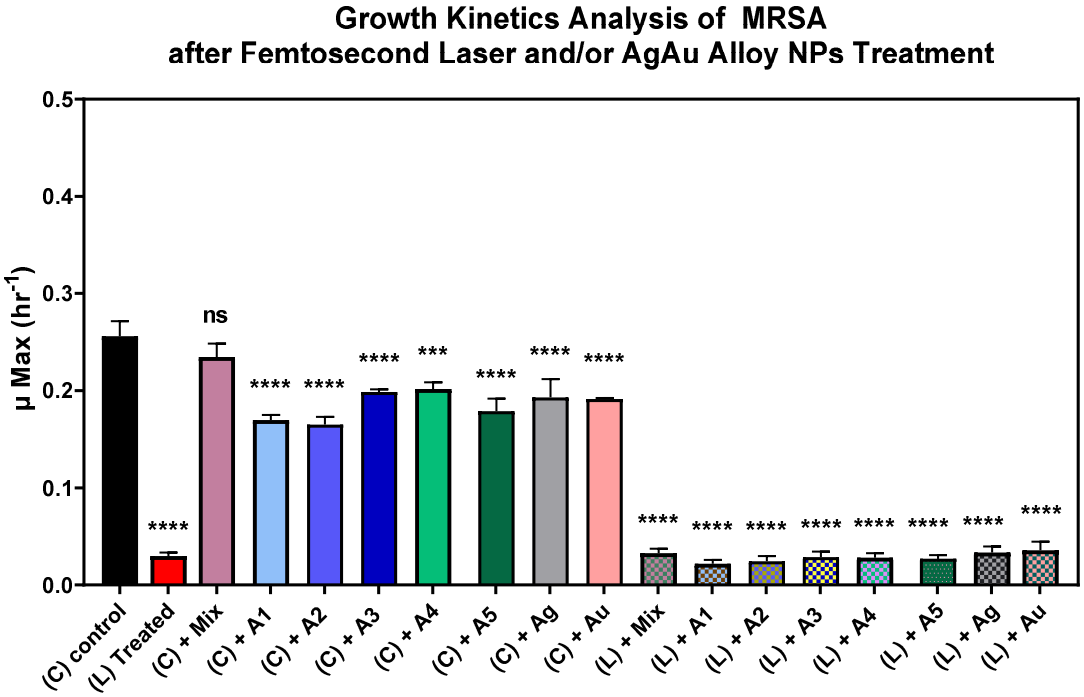

Figure 9: The bar graph illustrates the growth kinetics of methicillin-resistant Staphylococcus aureus (MRSA), comparing the log-phase growth rate kinetics of the control culture (C) with bacterial cultures subjected to various treatments. These treatments include femtosecond laser exposure (L), Ag/Au alloy NPs at different preparations (A1, A2, A3, A4, A5), Ag NPs, Au NPs, or Ag/Au mixture. The femtosecond laser treatment was performed at a wavelength of 400 nm, with an average power of 50 mW for 15 minutes. The cultures were exposed to five samples of Ag/Au alloy NPs: sample (A1) prepared at 500 mW for 15 min., sample (A2) prepared at 700 mW for 15 min., sample (A3) prepared at 900 mW for 15 min., sample (A4) prepared at 700 mW for 5 min., and sample (A5) prepared at 700 mW for 30 min. Significance was tested by ANOVA followed by the Tukey test (** P < 0.0001, *** P < 0.001).**

Our findings suggest that combining femtosecond laser and Ag/Au alloy NPs might greatly inhibit bacterial growth, potentially minimizing their harmful impacts in many scenarios. Overall, femtosecond laser irradiation and Ag/Au alloy nanoparticles demonstrated antimicrobial activity against MRSA, primarily through a "contact-killing" mechanism, consistent with observations reported in previous studies [49-51].

Using Ag/Au alloy NPs as an alternative antibacterial modality is still a trade of between the higher effects with increasing concentration and the safety concerns of this approach even with PLAL synthesis method that is why research proposals like preparation of alloy nanoparticles are being investigated to mask the toxicity while enabling the effect to take place [52,53].

Recent advancements in artificial intelligence (AI) have further enhanced the potential of nanotechnology by enabling predictive modeling, optimizing synthesis protocols, and accelerating discovery cycles [54] These capabilities may contribute significantly to future research focused on fine-tuning the optical, morphological, and antimicrobial features of bimetallic nanoparticles.

4. Conclusions

These results unlocked a new perception of synthesizing Ag/Au alloy nanoparticles via the laser ablation technique and their potential application in treating various ocular infections. Our results reveal that these alloys exhibit antibacterial activity against bacteria, either independently at higher concentrations or in synergy with 400 nm femtosecond laser treatment. However, the safety profile and enduring effects of Ag/Au alloy nanoparticles on the human body remain critical challenges, emphasizing the need for ongoing research into innovative or improved nanoparticle production methods.

Funding: This research received no external funding.

Data Availability Statement: Not applicable.

Conflicts of Interest: The authors declare no conflict of interest.

References

1. Teweldemedhin, M.; Gebreyesus, H.; Atsbaha, A.H.; Asgedom, S.W.; Saravanan, M. Bacterial profile of ocular infections: a systematic review. *BMC ophthalmology* **2017**, *17*, 1-9.
2. Long, C.; Liu, B.; Xu, C.; Jing, Y.; Yuan, Z.; Lin, X. Causative organisms of post-traumatic endophthalmitis: a 20-year retrospective study. *BMC ophthalmology* **2014**, *14*, 1-7.
3. Teweldemedhin, M.; Saravanan, M.; Gebreyesus, A.; Gebreegziabiher, D. Ocular bacterial infections at Quiha Ophthalmic Hospital, Northern Ethiopia: an evaluation according to the risk factors and the antimicrobial susceptibility of bacterial isolates. *BMC infectious diseases* **2017**, *17*, 1-11.
4. Shimizu, Y.; Toshida, H.; Honda, R.; Matsui, A.; Ohta, T.; Asada, Y.; Murakami, A. Prevalence of drug resistance and culture-positive rate among microorganisms isolated from patients with ocular infections over a 4-year period. *Clinical Ophthalmology* **2013**, 695-702.
5. Vaziri, K.; Schwartz, S.G.; Kishor, K.; Flynn Jr, H.W. Endophthalmitis: state of the art. *Clinical ophthalmology* **2015**, 95-108.
6. Khosravi, A.; Mehdinejad, M.; Heidari, M. Bacteriological findings in patients with ocular infection and antibiotic susceptibility patterns of isolated pathogens. *Singapore medical journal* **2007**, *48*, 741.
7. Sarmah, P.; Shenoy, P. Profile of microbial isolates in ophthalmic infections and antibiotic susceptibility of the bacterial isolates: a study in an eye care hospital, Bangalore. *Journal of clinical and diagnostic research: JCDR* **2014**, *8*, 23.
8. Gao, W.; Zhang, L. Nanomaterials arising amid antibiotic resistance. *Nature Reviews Microbiology* **2021**, *19*, 5-6.
9. Makabenta, J.M.V.; Nabawy, A.; Li, C.-H.; Schmidt-Malan, S.; Patel, R.; Rotello, V.M. Nanomaterial-based therapeutics for antibiotic-resistant bacterial infections. *Nature Reviews Microbiology* **2021**, *19*, 23-36.
10. Libralato, G.; Galdiero, E.; Falanga, A.; Carotenuto, R.; De Alteriis, E.; Guida, M. Toxicity effects of functionalized quantum dots, gold and polystyrene nanoparticles on target aquatic biological models: a review. *Molecules* **2017**, *22*, 1439.
11. Gu, X.; Xu, Z.; Gu, L.; Xu, H.; Han, F.; Chen, B.; Pan, X. Preparation and antibacterial properties of gold nanoparticles: A review. *Environmental Chemistry Letters* **2021**, *19*, 167-187.
12. Preeti; Radhakrishnan, V.; Mukherjee, S.; Mukherjee, S.; Singh, S.P.; Prasad, T. ZnO quantum dots: broad Spectrum Microbicidal agent against multidrug resistant Pathogens E. Coli and C. albicans. *Frontiers in Nanotechnology* **2020**, *2*, 576342.
13. Shanmugapriya, K.; Kang, H.W. Engineering pharmaceutical nanocarriers for photodynamic therapy on wound healing. *Materials Science and Engineering: C* **2019**, *105*, 110110.
14. Ahmed, E.; El-Gendy, A.O.; Hamblin, M.R.; Mohamed, T. The effect of femtosecond laser irradiation on the growth kinetics of Staphylococcus aureus: An in vitro study. *Journal of Photochemistry and Photobiology B: Biology* **2021**, *221*, 112240.
15. El-Gendy, A.O.; Samir, A.; Ahmed, E.; Enwemeka, C.S.; Mohamed, T. The antimicrobial effect of 400 nm femtosecond laser and silver nanoparticles on gram-positive and gram-negative bacteria. *Journal of Photochemistry and Photobiology B: Biology* **2021**, *223*, 112300.
16. El-Gendy, A.O.; Nawaf, K.T.; Ahmed, E.; Samir, A.; Hamblin, M.R.; Hassan, M.; Mohamed, T. Preparation of zinc oxide nanoparticles using laser-ablation technique: Retinal epithelial cell (ARPE-19) biocompatibility and antimicrobial activity when activated with femtosecond laser. *Journal of Photochemistry and Photobiology B: Biology* **2022**, *234*, 112540.
17. El-Gendy, A.O.; Obaid, Y.; Ahmed, E.; Enwemeka, C.S.; Hassan, M.; Mohamed, T. The antimicrobial effect of gold quantum dots and femtosecond laser irradiation on the growth kinetics of common infectious eye pathogens: an in vitro study. *Nanomaterials* **2022**, *12*, 3757.
18. Hassan, B.A.; Lawi, Z.K.K.; Banoon, S.R. Detecting the activity of silver nanoparticles, pseudomonas fluorescens and Bacillus circulans on inhibition of aspergillus Niger growth isolated from moldy orange fruits. **2020**.

19. Sun, L.; Luan, W.; Shan, Y.J.J.N.r.l. A composition and size controllable approach for Au-Ag alloy nanoparticles. **2012**, *7*, 1-6.
20. Mulvaney, P.J.L. Surface plasmon spectroscopy of nanosized metal particles. **1996**, *12*, 788-800.
21. Tyurnina, A.E.; Shur, V.Y.; Kozin, R.V.; Kuznetsov, D.K.; Mingaliev, E.A. Synthesis of stable silver colloids by laser ablation in water. In Proceedings of the Fundamentals of Laser-Assisted Micro-and Nanotechnologies 2013, 2013; pp. 128-135.
22. Mafuné, F.J.C.p.l. Structure diagram of gold nanoparticles in solution under irradiation of UV pulse laser. **2004**, *397*, 133-137.
23. Aldujaili, N.H.; Banoon, S.R. ANTIBACTERIAL CHARACTERIZATION OF TITANIUM NANOPARTICLES NANOSYNTHESIZED BY STREPTOCOCCUS THERMOPHILUS. *Periódico Tchê Química* **2020**, *17*.
24. Qayyum, H.; Amin, S.; Ahmed, W.; Mohamed, T.; Rehman, Z.U.; Hussain, S.J.J.o.M.L. Laser-based two-step synthesis of Au-Ag alloy nanoparticles and their application for surface-enhanced Raman spectroscopy (SERS) based detection of rhodamine 6G and urea nitrate. **2022**, *365*, 120120.
25. Neumeister, A.; Jakobi, J.; Rehbock, C.; Moysig, J.; Barcikowski, S.J.P.C.C.P. Monophasic ligand-free alloy nanoparticle synthesis determinants during pulsed laser ablation of bulk alloy and consolidated microparticles in water. **2014**, *16*, 23671-23678.
26. Gal, G.; Monsa, Y.; Ezersky, V.; Bar, I.J.R.a. Alloying copper and palladium nanoparticles by pulsed laser irradiation of colloids suspended in ethanol. **2018**, *8*, 33291-33300.
27. Kuladeep, R.; Jyothi, L.; Alee, K.S.; Deepak, K.; Rao, D.N.J.O.M.E. Laser-assisted synthesis of Au-Ag alloy nanoparticles with tunable surface plasmon resonance frequency. **2012**, *2*, 161-172.
28. Ghorbani, J.; Rahban, D.; Aghamiri, S.; Teymouri, A.; Bahador, A. Photosensitizers in antibacterial photodynamic therapy: An overview. *Laser therapy* **2018**, *27*, 293-302.
29. Cassidy, C.M.; Tunney, M.M.; McCarron, P.A.; Donnelly, R.F. Drug delivery strategies for photodynamic antimicrobial chemotherapy: from benchtop to clinical practice. *J Photochem Photobiol B* **2009**, *95*, 71-80, doi:10.1016/j.jphotobiol.2009.01.005.
30. Samaneh, R.; Ali, Y.; Mostafa, J.; Mahmud, N.A.; Zohre, R. Laser therapy for wound healing: A review of current techniques and mechanisms of action. *Biosci, Biotech Res Asia* **2015**, *12*, 217-223.
31. Amiri, M.; Etemadifar, Z.; Daneshkazemi, A.; Nateghi, M. Antimicrobial effect of copper oxide nanoparticles on some oral bacteria and candida species. *Journal of dental biomaterials* **2017**, *4*, 347.
32. Vincent, M.; Duval, R.E.; Hartemann, P.; Engels-Deutsch, M. Contact killing and antimicrobial properties of copper. *Journal of applied microbiology* **2018**, *124*, 1032-1046.
33. Adamczyk, Z.; Oćwieja, M.; Mrowiec, H.; Walas, S.; Lupa, D. Oxidative dissolution of silver nanoparticles: A new theoretical approach. *Journal of Colloid and Interface Science* **2016**, *469*, 355-364.
34. Peretyazhko, T.S.; Zhang, Q.; Colvin, V.L. Size-controlled dissolution of silver nanoparticles at neutral and acidic pH conditions: kinetics and size changes. *Environmental science & technology* **2014**, *48*, 11954-11961.
35. Moschini, E.; Colombo, G.; Chirico, G.; Capitani, G.; Dalle-Donne, I.; Mantecca, P. Biological mechanism of cell oxidative stress and death during short-term exposure to nano CuO. *Scientific Reports* **2023**, *13*, 2326.
36. Hammer, B.; Norskov, J.K. Why gold is the noblest of all the metals. *Nature* **1995**, *376*, 238-240.
37. Okkeh, M.; Bloise, N.; Restivo, E.; De Vita, L.; Pallavicini, P.; Visai, L. Gold nanoparticles: can they be the next magic bullet for multidrug-resistant bacteria? *Nanomaterials* **2021**, *11*, 312.
38. Cheng, G.; Li, B. Nanoparticle-based photodynamic therapy: New trends in wound healing applications. *Materials Today Advances* **2020**, *6*, 100049.
39. Pajerski, W.; Ochonska, D.; Brzychczy-Wloch, M.; Indyka, P.; Jarosz, M.; Golda-Cepa, M.; Sojka, Z.; Kotarba, A. Attachment efficiency of gold nanoparticles by Gram-positive and Gram-negative bacterial strains governed by surface charges. *Journal of Nanoparticle Research* **2019**, *21*, 1-12.
40. Wang, L.; Hu, C.; Shao, L. The antimicrobial activity of nanoparticles: present situation and prospects for the future. *International journal of nanomedicine* **2017**, 1227-1249.
41. Nagy, A.; Harrison, A.; Sabbani, S.; Munson Jr, R.S.; Dutta, P.K.; Waldman, W.J. Silver nanoparticles embedded in zeolite membranes: release of silver ions and mechanism of antibacterial action. *International journal of nanomedicine* **2011**, 1833-1852.
42. Gurunathan, S.; Han, J.W.; Dayem, A.A.; Eppakayala, V.; Kim, J.-H. Oxidative stress-mediated antibacterial activity of graphene oxide and reduced graphene oxide in Pseudomonas aeruginosa. *International journal of nanomedicine* **2012**, 5901-5914.
43. Leung, Y.H.; Ng, A.M.; Xu, X.; Shen, Z.; Gethings, L.A.; Wong, M.T.; Chan, C.M.; Guo, M.Y.; Ng, Y.H.; Djurišić, A.B. Mechanisms of antibacterial activity of MgO: non-ROS mediated toxicity of MgO nanoparticles towards Escherichia coli. *Small* **2014**, *10*, 1171-1183.
44. Panicker, S.; Ahmady, I.; Han, C.; Chehimi, M.; Mohamed, A. On demand release of ionic silver from gold-silver alloy nanoparticles: fundamental antibacterial mechanisms study. *Materials Today Chemistry* **2020**, *16*, 100237.
45. Ahmed, E.; El-Gendy, A.O.; Moniem Radi, N.A.; Mohamed, T. The bactericidal efficacy of femtosecond laser-based therapy on the most common infectious bacterial pathogens in chronic wounds: An in vitro study. *Lasers in Medical Science* **2021**, *36*, 641-647.
46. Hurdle, J.G.; O'neill, A.J.; Chopra, I.; Lee, R.E. Targeting bacterial membrane function: an underexploited mechanism for treating persistent infections. *Nature Reviews Microbiology* **2011**, *9*, 62-75.

47. Hayden, S.C.; Zhao, G.; Saha, K.; Phillips, R.L.; Li, X.; Miranda, O.R.; Rotello, V.M.; El-Sayed, M.A.; Schmidt-Krey, I.; Bunz, U.H. Aggregation and interaction of cationic nanoparticles on bacterial surfaces. *Journal of the American Chemical Society* **2012**, *134*, 6920-6923.
48. Simon-Deckers, A.; Loo, S.; Mayne-L'hermite, M.; Herlin-Boime, N.; Menguy, N.; Reynaud, C.; Gouget, B.; Carrière, M. Size-, composition-and shape-dependent toxicological impact of metal oxide nanoparticles and carbon nanotubes toward bacteria. *Environmental science & technology* **2009**, *43*, 8423-8429.
49. Gonçalves, R.A.; Ku, J.W.; Zhang, H.; Salim, T.; Oo, G.; Zinn, A.A.; Boothroyd, C.; Tang, R.M.; Gan, C.L.; Gan, Y.-H. Copper-nanoparticle-coated fabrics for rapid and sustained antibacterial activity applications. *ACS Applied Nano Materials* **2022**, *5*, 12876-12886.
50. Fazal, A.; Ara, S.; Ishaq, M.T.; Sughra, K. Green fabrication of copper oxide nanoparticles: a comparative antibacterial study against gram-positive and gram-negative bacteria. *Arabian Journal for Science and Engineering* **2022**, *47*, 523-533.
51. Azam, A.; Ahmed, A.S.; Oves, M.; Khan, M.S.; Memic, A. Size-dependent antimicrobial properties of CuO nanoparticles against Gram-positive and-negative bacterial strains. *International journal of nanomedicine* **2012**, 3527-3535.
52. Kirtane, A.R.; Verma, M.; Karandikar, P.; Furin, J.; Langer, R.; Traverso, G. Nanotechnology approaches for global infectious diseases. *Nature Nanotechnology* **2021**, *16*, 369-384.
53. Fries, C.N.; Curvino, E.J.; Chen, J.-L.; Permar, S.R.; Fouda, G.G.; Collier, J.H. Advances in nanomaterial vaccine strategies to address infectious diseases impacting global health. *Nature Nanotechnology* **2021**, *16*, 1-14.
54. Hassan, S.A.-D.H.; Almaliki, M.N.S.; Hussein, Z.A.; Albehadili, H.M.; Rabeea Banoon, S.; Abboodi, A.; Al-Saady, M. Development of nanotechnology by artificial intelligence: a comprehensive review. *Journal of Nanostructures* **2023**, *13*, 915-932.